Relating Friction Velocity to Spectral Wave Parameters

WILLIAM PERRIE AND BECHARA TOULANY

*Physical and Chemical Sciences, Scotia–Fundy Region, Department of Fisheries and Oceans,
Bedford Institute of Oceanography, Dartmouth, Nova Scotia, Canada*

ABSTRACT

Field experiments, in the years since the JONSWAP results, have established fetch- and duration-limited relations for wave parameters such as total energy E_0, peak frequency f_p, and the Phillips α coefficient. The Canadian Atlantic Storms Program (CASP) Experiment of 1986 also found that the wind speed profile appropriate for the fetch-limited wave relations is a function of fetch, due to the change in surface roughness at the shoreline. Moreover, the fetch-limited wave relations may be altered by assuming differing wind speed variations with fetch. Inverting accepted fetch-limited wave relations, the authors infer a fetch-limited relation for wind speed (or friction velocity) in terms of spectral wave parameters such as wave age. These relations are verified from measurements collected during CASP.

1. Introduction

Considerable effort has been directed to understanding the coupling between the wave boundary layer (the lower part of the atmospheric boundary layer above the sea) and ocean surface waves in recent years. This is partly motivated by the growing archive of remotely sensed scatterometer wind observations from the *ERS-1* satellite. These wind observations are obtained from algorithms that are optimized such that the wind speeds they report, $\mathcal{U}_{scat}$, are a best fit to data $\mathcal{U}_{obs}$. Typically, as implemented by Woiceshyn and Janssen (1991) and Janssen and Woiceshyn (1991), the data $\mathcal{U}_{obs}$ is assumed to have the form

$$\mathcal{U}_{obs} \approx \text{const } \mathcal{C}_p / \mathcal{U}^*, \qquad (1.1)$$

where $\mathcal{C}_p$, the phase speed of the wave spectra at the peak frequency f_p, and $\mathcal{U}^*$, the friction velocity at some reference level such as 10 m, are obtained from reliable wave and atmospheric model outputs. There are potential problems in this procedure. First, the wave and atmospheric models may have biases in the values they report for $\mathcal{C}_p$ and $\mathcal{U}^*$. Biases follow from the usual collection of assumptions that constitute the models, such as the parameterizations for dissipation, for the coupling of wind to waves and for the energy transfer due to nonlinear wave–wave interactions. Second, the functional form expressed in Eq. (1.1) relating wind speed to wave parameters may not be complete, which is the concern of our paper.

The coupling between the wave boundary layer and ocean surface waves has been modeled by Chalikov (1993), Chalikov and Belevich (1995), Janssen (1991), Janssen (1989), Jenkins (1992), and others. Detailed models have resulted, showing the manner in which the wave boundary layer is directly influenced by surface waves. In one dimension (duration-limited conditions), Chalikov and Belevich (1993) estimate the variation of the drag coefficient C_d as approximately

$$\ln C_d = -6.460 + 0.102\Omega + 0.009\Omega^2$$

$$+ (0.311 + 0.055\Omega + 0.006\Omega^2)R$$

$$+ (0.032 + 0.011\Omega + 0.001\Omega^2)R^2, \qquad (1.2)$$

where $\Omega \equiv \mathcal{U}/\mathcal{C}_p$ is inverse wave age, $\mathcal{U}$ is the wind speed at a reference height z, and $R \equiv \ln(\mathcal{U}^2/gz)$ is related to inverse dimensionless height $\mathcal{U}^2/gz$. In principle, given observations of C_d at a given location, Eq. (1.2) can be inverted and the wind speed $\mathcal{U}$ expressed in terms of wave parameters:

$$\mathcal{U} = \mathcal{U}(C_d, gz, \mathcal{C}_p). \qquad (1.3)$$

The relation corresponding to (1.3) for fetch-limited observations in two dimensions has thus far not been explicitly derived. In this paper, we derive formulas for wind speed and friction velocity as functions of wave parameters, starting from empirical fetch-limited relations based on observations. We verify the resultant formulas with observations of the fetch-limited variation of wind speed.

It has recently been suggested by Marsden and Juszko (1989) that a quantity that they denote as *wave slope variance* may be used to calculate surface wind speeds. They looked at time series collected from a

Corresponding author address: William Perrie, Bedford Institute of Oceanography, P.O. Box 1006, Dartmouth, Nova Scotia B2Y 4A2 Canada.

directional wave buoy in open ocean conditions on the Grand Banks of Newfoundland and were able to find high correlations between directional wave buoy measurements of wave slope variance and surface wind speed. The directional wave buoy measures components of wave slope energy, denoted as $\langle k^2 \rangle E_0$, where $\langle k^2 \rangle$ is the mean squared wavenumber and E_0 the total energy. Section 2 shows that measured values for $\langle k^2 \rangle E_0$ may be related to the Phillips (1958, 1985) α coefficient. Hasselmann et al. (1973), Perrie and Toulany (1990), and others demonstrated that α is a slowly varying measure of spectral maturity, obeying fetch- and duration-limited growth relations analogous to those of total energy E_0 and peak frequency f_p. Moreover, friction velocity $\mathcal{U}^*$ (or wind speed $\mathcal{U}$) is used in the computation of α. The variation of $\mathcal{U}^*$ with fetch X reported by Smith and MacPherson (1987) contributes to the overall evolution of α with fetch X. Inversion of the $\alpha - \mathcal{U}^* - X$ relation therefore leads to a formulation for friction velocity $\mathcal{U}^*$ in terms of α and fetch X. However, the fetch X relation for α is related to the fetch relations for total energy E_0 and peak frequency f_p, as shown in Hasselmann et al. (1973), Resio and Perrie (1989), Perrie and Toulany (1990), and others. Therefore, we may express friction velocity $\mathcal{U}^*$ (and wind speed $\mathcal{U}$) in terms of fetch X (or wave age $\mathcal{C}_p/\mathcal{U}^*$) and wave slope variance $\langle k^2 \rangle E_0$.

Verification of the present analysis considers the two-dimensional directional wave spectra recorded by wave buoys during the Canadian Atlantic Storms Program (CASP) experiment of 1986. A brief overview of the CASP experiment, data, and relevant analyses is presented in section 3. The directional wave spectra collected during CASP were measured by three (WAVEC) pitch–roll wave buoys moored in 25-m, 50-m, and 100-m of water in a line orthogonal from the coastline at 5 km, 15 km, and 30 km from the shoreline, as shown in Fig. 1. A meteorological buoy at the seaward end of the wave buoy array measured wind speed and direction. Therefore, conditions when the wind is onshore may be clearly distinguished from conditions when it is offshore. Furthermore, conditions in which the directions of the high frequency spectral wave components, measured by the wave buoys, have relaxed to the wind direction may also be discerned, as shown in section 4.

Onshore wind situations are presented in section 5. In this case, the wind speed $\mathcal{U}$ is shown to correlate well with wave slope $\langle k^2 \rangle E_0$. Section 6 considers fetch-limited situations corresponding to offshore winds. In the latter case, wind speed $\mathcal{U}$ is first correlated with wave slope $\langle k^2 \rangle E_0$ at the outermost wave buoy, where measurements are available. Corresponding estimates are made relating $\mathcal{U}$ and $\langle k^2 \rangle E_0$ at the other two wave buoys, using relations derived in section 2. Knowing the wave slope $\langle k^2 \rangle E_0$ dependence on fetch X then allows estimates for the wind speed $\mathcal{U}$ (and, implicitly, the friction velocity $\mathcal{U}^*$) as a function of fetch X (or

wave age $\mathcal{C}_p/\mathcal{U}^*$). Results are compared to Smith and MacPherson (1987).

2. Relating wave slope to wind speed

To simplify notation, we define the spectral average of any function $\mathcal{F}$ as

$$\langle \mathcal{F} \rangle \equiv \frac{1}{E_0} \int_{f_s}^{f_N} \int_0^{2\pi} \mathcal{F} \cdot E(f, \theta) d\theta df, \quad (2.1)$$

where $E(f, \theta)$ is the two-dimensional wave spectrum, f_N the Nyquist frequency for the wave buoys, and f_s the frequency that separates swell from local wind-generated waves. The north–south wave slope energy E_2 for a given directional buoy, as derived by Longuet-Higgins et al. (1963), is

$$E_2 = \langle k^2 \cos^2\theta \rangle E_0, \quad (2.2)$$

the east–west wave slope energy E_3 is

$$E_3 = \langle k^2 \sin^2\theta \rangle E_0, \quad (2.3)$$

and, finally, the total wave slope energy $E_2 + E_3$ is

$$E_2 + E_3 = \langle k^2 \rangle E_0. \quad (2.4)$$

These will be related to the Phillips (1958, 1985) α coefficient.

The determination of α and its variation, as the wave spectra grow and evolve toward maturity, is a key element in the study of CASP data by Perrie and Toulany (1990). They evaluated α by averaging over the high frequency equilibrium range of the one-dimensional energy spectrum $E(f)$, following Donelan et al. (1985),

$$\alpha = \frac{(2\pi)^3}{g\mathcal{U}^*} \frac{1}{(f_N - 1.5f_p)} \int_{1.5f_p}^{f_N} f^4 E(f) \exp(f_p^4/f^4) df, \quad (2.5)$$

where g is the acceleration due to gravity. Perrie and Toulany (1990) derived fetch relations in terms of dimensionless peak frequency f_p^* and dimensionless fetch X^* from the CASP observations—for example,

$$\left. \begin{array}{l} \alpha = \mathcal{A}(f_p^*)^a \\ f_p^* = \mathcal{B}(X^*)^b \end{array} \right\}, \quad (2.6)$$

where $\mathcal{A}$, a, $\mathcal{B}$, and b are constants for CASP data. Dimensionless peak frequency and dimensionless fetch are defined by

$$\left. \begin{array}{l} f_p^* = f_p \mathcal{U}^*/g \\ X^* = Xg/\mathcal{U}^{*2} \end{array} \right\}, \quad (2.7)$$

where friction velocity $\mathcal{U}^*$ is related to wind speed $\mathcal{U}$ at a reference height such as 10 m through a drag coefficient C_d:
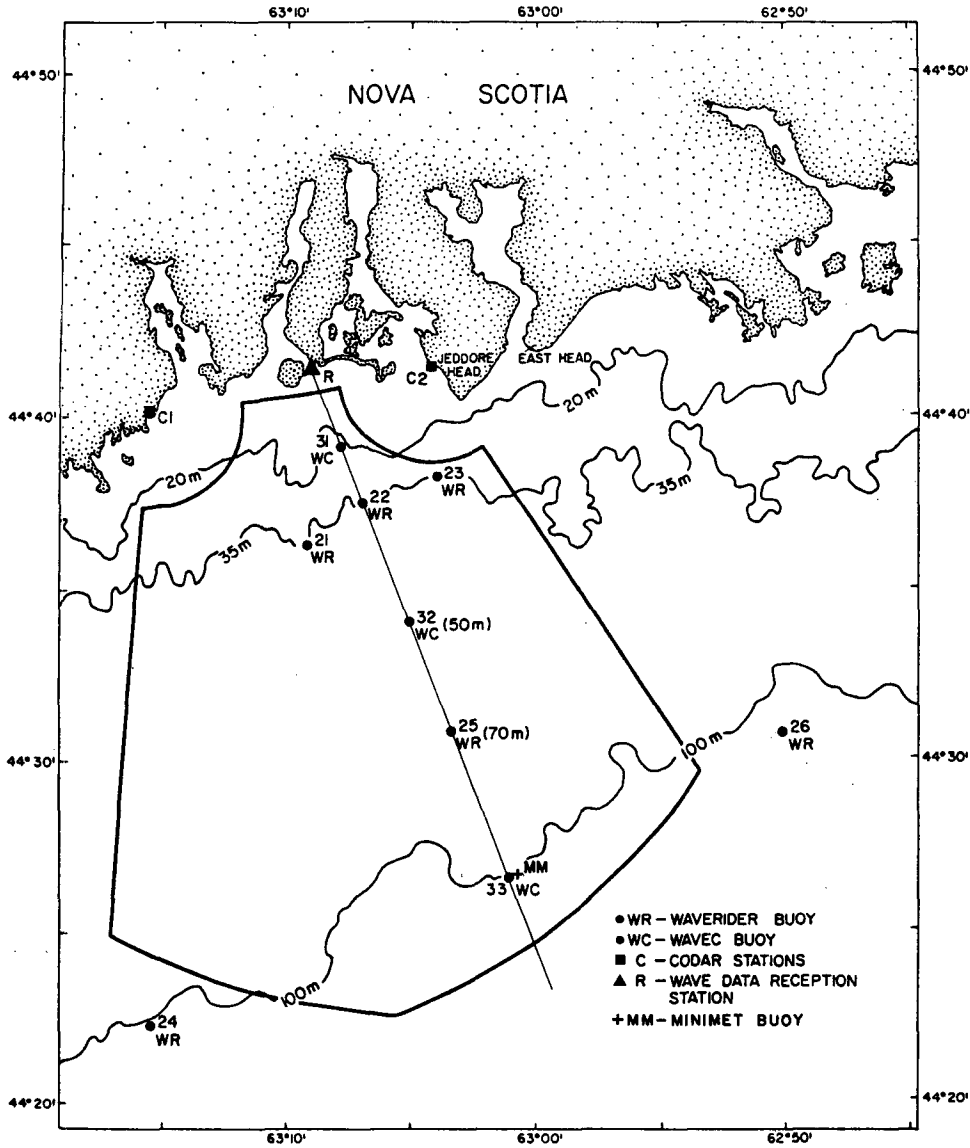
FIG. 1. The CASP wave buoy array showing shoreline mesonet meteorological stations at Martinique Beach, Fox Point, and Clam Harbour and ground-based radar (CODAR).

$$\mathcal{U}* = \mathcal{U}\sqrt{C_d}. \qquad (2.8)$$

Recognizing that $\exp(f_p^4/f^4) \approx 1$ for $1.5 f_p < f < f_N$, we make the approximation

$$\int_{1.5f_p}^{f_N} f^4 E(f) \exp(f_p^4/f^4) df \approx \int_{1.5f_p}^{f_N} f^4 E(f) df \qquad (2.9)$$

and we introduce a coefficient $\mathcal{J}$

$$\mathcal{J} = \frac{\displaystyle\int_{1.5f_p}^{f_N} f^4 E(f) df}{\displaystyle\int_{f_s}^{f_N} f^4 E(f) df}. \qquad (2.10)$$

Using the averaging notation of Eq. (2.1), this may be expressed as the ratio

$$\mathcal{J} = \frac{\langle f^4 \rangle_{\text{eq.ra.}} (E_0)_{\text{eq.ra.}}}{\langle f^4 \rangle E_0}, \qquad (2.11)$$

where subscript "eq.ra." denotes evaluation of E_0 and $\langle f^4 \rangle$ over the equilibrium range $[1.5 f_p, f_N]$. Arguments that $\mathcal{J}$ is approximately constant are presented in the Appendix.

Returning to the expression for α in Eq. (2.5), we substitute Eqs. (2.9)–(2.11) and obtain

$$\alpha = \frac{(2\pi)^3}{g\mathcal{U}*} \frac{1}{(f_N - 1.5f_p)} \mathcal{J} E_0 \langle f^4 \rangle \qquad (2.12)$$

or, alternately, using the deep water dispersion relation,

$$\alpha = \frac{g}{2\pi \mathcal{U}^*(f_N - 1.5 f_p)} \mathcal{J} E_0 \langle k^2 \rangle. \qquad (2.13)$$

Therefore, in terms of $E_2 + E_3$ given in Eq. (2.4), we may write

$$\alpha = \frac{g}{2\pi \mathcal{U}^* f_N (1 - 1.5 f_p / f_N)} \mathcal{J}(E_2 + E_3). \qquad (2.14)$$

Substituting the fetch relation given in Eq. (2.6), we obtain a friction velocity $\mathcal{U}^*$ relation in terms of wave slope and f_p^*,

$$\mathcal{U}^* = \frac{3 g f_p^*}{2 f_N} + \frac{g \mathcal{J}}{2 \pi \mathcal{A}(f_p^*)^a f_N} s, \qquad (2.15)$$

where s represents wave slope $E_2 + E_3$. Replacing friction velocity by wind speed through Eq. (2.8), we may write

$$\mathcal{U} = \frac{3 g f_p^*}{2 f_N C_d^{1/2}} + \frac{g \mathcal{J}}{2 \pi \mathcal{A}(f_p^*)^a f_N C_d^{1/2}} s. \qquad (2.16)$$

Assuming the usual partition of the two-dimensional energy spectrum $E(f, \theta)$ into an angular spreading function $\Lambda(\theta)$ and the one-dimensional spectrum $E(f)$, following Hasselmann and Hasselmann (1981) and others, we write

$$E(f, \theta) = \Lambda(\theta) E(f), \qquad (2.17)$$

which is normalized to satisfy $\int_0^{2\pi} \Lambda(\theta) d\theta = 1$. The directional components of Eqs. (2.2) and (2.3) may therefore be written as

$$\left. \begin{array}{l} \langle k^2 \sin^2 \theta \rangle = \mathcal{P}_s \langle k^2 \rangle \\ \langle k^2 \cos^2 \theta \rangle = \mathcal{P}_c \langle k^2 \rangle \end{array} \right\}, \qquad (2.18)$$

where $\mathcal{P}_s$ and $\mathcal{P}_c$ are constants. It follows that the north–south E_2 and east–west E_3 components of spectral wave slope in Eqs. (2.2) and (2.3) lead to expressions for wind speed in terms of spectral wave parameters that are analogous to Eq. (2.16).

The wave slope energy (E_2, E_3, or $E_2 + E_3$) as described above actually measures a portion of the mean square slope. Moreover, it is evident from Cox and Munk (1954a,b) that part of the mean square slope is in the short waves and cannot be sensed by the buoys. This is unimportant for the analysis considered here. From Eq. (2.5), it is important that E_2, E_3, and $E_2 + E_3$ constitute measurements leading to reliable estimates of α. In that regard, it is not essential that the nyquist frequency f_N of the buoys extend to the high frequencies investigated by Cox and Munk (1954a,b). It is only important that the wave buoy measurements extend to high enough frequency bands in the equilibrium range of the spectrum so that a stable average be generated from Eq. (2.5) for the determination of α. From the analysis by Perrie and Toulany (1990), it is

clear that this is achieved. Correlation coefficients as high as 0.73 were obtained for relating α to wave age $\mathcal{C}_p / \mathcal{U}^*$. In accurately evaluating α from Eq. (2.5), Perrie and Toulany (1990) found that it is only necessary to require that f_N be at least five frequency bands, of width 0.005 Hz, above $1.5 f_p$.

Replacing coefficients $3 g f_p^* / (2 f_N C_d^{1/2})$ and $g \mathcal{J} / [2 \pi \mathcal{A}(f_p^*)^a f_N C_d^{1/2}]$ by $\mathcal{C}_x$ and $\mathcal{D}_x$ in Eq. (2.16), we may represent the wind speed at wave buoys, denoted WAVEC33, WAVEC32, and WAVEC31 in Fig. 1, as

$$\left. \begin{array}{l} \mathcal{U}_3 = \mathcal{C}_3 + \mathcal{D}_3 s \\ \mathcal{U}_2 = \mathcal{C}_2 + \mathcal{D}_2 s \\ \mathcal{U}_1 = \mathcal{C}_1 + \mathcal{D}_1 s \end{array} \right\}. \qquad (2.19)$$

Because wind and wave measurements are both made at the outermost wave buoy WAVEC33, coefficients $\mathcal{C}_3$ and $\mathcal{D}_3$ are therefore determined. From Eq. (2.16) and the fetch relation for peak frequency (2.6), it follows that

$$\left. \begin{array}{l} \mathcal{C}_2 = \mathcal{C}_3 (X_2/X_3)^b (C_{d2}/C_{d3})^{-1/2-b} \Gamma_{23}^{-2b} \\ \mathcal{D}_2 = \mathcal{D}_3 (X_2/X_3)^{-ab} (C_{d2}/C_{d3})^{ab-1/2} \Gamma_{23}^{2ab} \end{array} \right\}, \qquad (2.20)$$

where $\Gamma_{23} \equiv \mathcal{U}_2 / \mathcal{U}_3$. The drag coefficient at the outermost buoy is denoted C_{d3} and at the middle buoy, C_{d2}. We do not assume that C_{d2} is the same as C_{d3}, unless specifically noted. The equation for Γ_{23} therefore has the form

$$\Gamma_{23} = \left(\mathcal{C}_3 \left(\frac{X_2}{X_3} \right)^b \left(\frac{C_{d2}}{C_{d3}} \right)^{-1/2-b} \Gamma_{23}^{-2b} \right.$$
$$\left. + \mathcal{D}_3 \left(\frac{X_2}{X_3} \right)^{-ab} \left(\frac{C_{d2}}{C_{d3}} \right)^{ab-1/2} \Gamma_{23}^{2ab} s \right) \mathcal{U}_3^{-1}, \qquad (2.21)$$

and a similar relation may be derived for $\Gamma_{13} \equiv \mathcal{U}_1 / \mathcal{U}_3$. Equation (2.21) may be solved iteratively.

Because the fetch relations from the CASP analysis of Perrie and Toulany (1990) are the basis for this paper, it is necessary to consider their formulations for drag coefficient. The simplest of these was the constant drag coefficient,

$$C_d |_{\text{const}} = 1.3 \times 10^{-3}. \qquad (2.22)$$

Perrie and Toulany (1990) also considered the open ocean long-fetch drag coefficient, from the stable tower experiment of Smith (1988) at the mouth of Halifax Harbour

$$C_d |_{\text{long fetch}} = C_d [\mathcal{U}, \Delta T]_{\text{long fetch}}, \qquad (2.23)$$

where ΔT is the difference between water and air temperature. Finally, they considered an approximation to the HEXOS (Humidity Experiment Over the Sea) drag coefficient results, showing a dependence on sea-

state maturity as reported by Smith and Anderson (1989),

$$C_d|_{\text{HEXOS}} = \begin{cases} C_d[\mathcal{U}, \Delta T]_{\text{long fetch}} \\ + (1.51 - 1.87\mathcal{C}_p/\mathcal{U}_c) \times 10^{-3}, \\ \qquad \text{when} \quad 0 < \mathcal{C}_p/\mathcal{U}_c < 0.81 \\ C_d[\mathcal{U}, \Delta T]_{\text{long fetch}}, \quad \text{otherwise,} \end{cases}$$

(2.24)

where $\mathcal{U}_c$ is the component wind velocity in the direction of the waves at f_p. We emphasize that this formulation is slightly at variance with the final HEXOS results reported by Smith et al. (1992). However, this formulation is implicit in the most consistent fetch relations resulting from the Perrie and Toulany (1990) analysis of the CASP data. Moreover, the HEXOS dataset was free of swell and it is unclear as to how associated C_d parameterizations should apply to swell-infested data of the CASP experiment. Recent measurements of drag coefficient in the presence of swell, by Dobson et al. (1994) during the Grand Banks ERS-1 Calibration/Validation Experiment are at variance with the HEXOS measurements.

As stated in Perrie and Toulany (1990), wave measurements in CASP were actually scaled by the wind, linearly averaged along the fetch from the shore to each of the wave buoys, exactly following the procedure of Dobson et al. (1989). This represents the ability of the waves to "remember" the wind all along the fetch. Scaling by the average wind along the fetch is only one way to represent this memory. Of course, for zero or infinite fetches, linearly averaged wind is the same as in situ wind, with the greatest discrepancies between in situ and linearly averaged wind occurring at about 15 km, the midpoint of the wave buoy array. It is important to note that in Eqs. (2.16) and (2.21), $\mathcal{U}$ is therefore understood to be the wind speed, linearly averaged from the shore to a particular wave buoy. Were we to use the Donelan et al. (1985) Lake Ontario parameterizations for fetch-limited growth, we would then understand $\mathcal{U}$ to denote in situ wind speed, as that is what was used to scale wave measurements in that experiment.

From the JONSWAP observations of Hasselmann et al. (1973), the Perrie and Toulany (1990) results, and many other field programs, both terms $3gf_p^*/(2f_N)$ and $g\mathcal{J}/(2\pi\alpha f_N)s$ in Eq. (2.15) vary with wave age. Thus, the evaluation of $3gf_p^*/(2f_N)$ and $g\mathcal{J}/(2\pi\alpha f_N)s$, as measured at the outermost wave buoy, will differ from corresponding values at the other two wave buoys. In fact, it may be shown numerically that ignoring Eq. (2.21) and simply attributing the calibration of wind speed with wave slope, as found at wave buoy WAVEC33, to the other wave buoys WAVEC32 or WAVEC31 constitutes an overestimate of wind speeds at WAVEC32 and WAVEC31.

3. The CASP Experiment

Figure 1 shows the array of directional (WAVEC) and heave (WAVERIDER) wave buoys deployed off the coast of Nova Scotia during the CASP Experiment, as presented by Dobson et al. (1989). Also shown are meteorological stations along the coast and a meteorological buoy (MINIMET) at the seaward end of the wave buoy array that recorded the wind speed and direction. The WAVEC buoys recorded the cross spectra between all pairs of raw time series data for heave energy E_0, north–south slope energy E_2, east–west slope energy E_3 from mid-January until late March 1986. Swell was always significant in the CASP wave spectra. Wind-generated sea spectra were separated from swell spectra as described in Dobson et al. (1989).

The wind profile for offshore winds was inferred from meteorological measurements at the coast, at the meteorological buoy, and from the aircraft measurements of Smith and MacPherson (1987). The boundary layer guidelines of Taylor and Lee (1984) were also applied. The fetch relations inferred by Perrie and Toulany (1990) assume the resultant wind speed profile. As discussed in section 2, wave measurements were scaled by this wind speed, linearly averaged from the shore to each wave buoy.

An extensive discussion of the observations recorded by a meteorological buoy appears in Dobson et al. (1989) and Hasse et al. (1978). Wind data can be biased because (i) the mean wind velocity measured at a given sensor height is reduced by the exponential height variation of the wave-induced fluctuations, (ii) the buoy moves with the water surface while the wave-induced streamline amplitude decreases with height, implying movement of the buoy sensor relative to the wave streamlines, and (iii) in an approximately logarithmic atmospheric boundary layer, measured wind speed is reduced because of the pitching motion of the buoy. The cumulative effect of these three errors on the accuracy of the winds measured by the meteorological buoy during CASP was an estimated error of about 2% as reported by Dobson et al. (1989), which is much less than other calibration errors.

To test the accuracy of the meteorological buoy (MINIMET) measurements, MINIMET winds were converted to a 10-m measurement height. The air temperature at the shoreline station on Martinique Beach and the sea temperature at the MINIMET, indicated in Fig. 1, were used to allow for atmospheric stability following Smith (1981). Comparison was made with the shoreline wind speeds recorded at the shoreline station. When winds were onshore and stationary (within ±50° of the offshore normal with no hourly changes >20%), MINIMET winds agreed with Martinique Beach winds to within 1.5% with standard error of 2.5%. For winds less than 25 m s^{-1}, this corresponds to a maximum error that is less than 1 m s^{-1}. Other calibrations were performed with routine meteorolog-
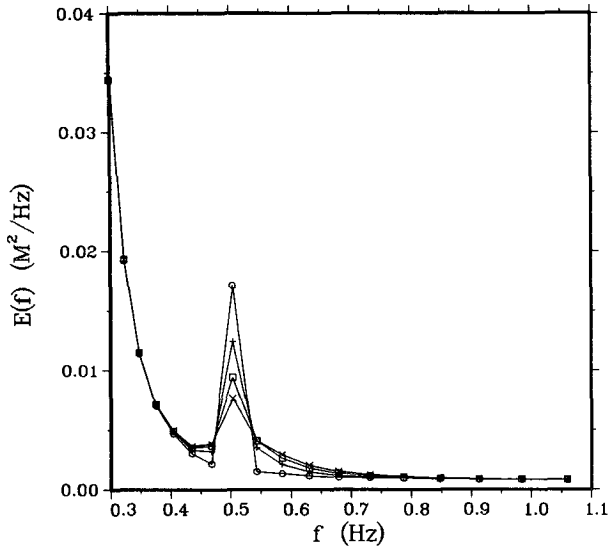
FIG. 2. Evolution of the energy spectrum in response to a 10X perturbation at $1.6f_p$, where the high frequency spectrum is denoted by -O-O- initially, by -+-+- after 1 min, by -□-□- after 2 min, and -X-X- after 3 min.

ical measurements at Shearwater Airport in Dartmouth, Nova Scotia, and laboratory calibrations before and after deployment. MINIMET sensors were estimated to have accuracies of ±4% in wind speed and ±2.5° in wind direction.

4. Wind direction

Later sections require knowing the wave direction of the equilibrium range frequency bands to ensure that the wave spectra have relaxed to the wind direction. In this section we consider correlations between the wind direction and the spectral wave directions in the high frequency bands. It is necessary to consider the behavior of all three WAVEC directional wave buoys to avoid situations where wind directions are changing and to show the extent to which all buoys are consistent. Moreover, deviations in the high frequency wave directions from the wind direction, due to the influence of the coastline, are also present. These deviations specify the directions at which *slanting fetch* or *alongshore* winds experience diffraction by the shoreline.

In separating swell from wind-generated waves, Dobson et al. (1989) found (illustrated in detail in their Fig. 4) that the region of the wave spectrum above about twice the spectral peak follows the shifting direction of the wind very closely. Computations of Resio and Perrie (1991) demonstrate that the response of nonlinear wave–wave interactions is very fast in this, the equilibrium region of the spectrum. As shown in Fig. 2, a 10 times perturbation at 1.6 times the spectral peak f_p is largely removed by the nonlinear transfer within 3 min. Perturbations in higher frequency bands

of the equilibrium region are erased in this amount of time.

A well-behaved wave direction, which is closely associated with the wind direction, may be computed by constructing the mean wave direction $\bar{\theta}$ for the upper equilibrium range (the region of the spectrum above 0.4 Hz or $1.5f_p$, whichever is higher)

$$\bar{\theta} = \frac{1}{\min[3.0f_p, f_N] - \max[0.4 \text{ Hz}, 1.5f_p]} \int_{\max[0.4 \text{ Hz}, 1.5f_p]}^{\min[3.0f_p, f_N]} \theta(f) df, \tag{4.1}$$

where θ is the wave direction at frequency f determined from the quadspectra between the heave signal and the north–south wave slope Q_{12}, and the heave signal and the east–west slope Q_{13}

$$\theta = \arctan\left(-\frac{Q_{13}}{Q_{12}}\right) \tag{4.2}$$

corrected for the magnetic declination. Angles defined by $+\frac{3}{2}\pi \leqslant \theta(f)$ and $\theta(f) \leqslant +\pi/2$ were specified as in the domain $-\pi/2 \leqslant \theta(f) \leqslant +\pi/2$, to correctly obtain a mean direction by averaging angles varying from $(2\pi)^-$ to 0^+. Nyquist frequency f_N is 0.64 Hz. This method avoids the 180° ambiguity encountered using raw time series data. Figure 3 compares the wind direction at the MINIMET with the wave direction as calculated from Eq. (4.1) for the outermost wave buoy, when estimates corresponding to wind speeds less than
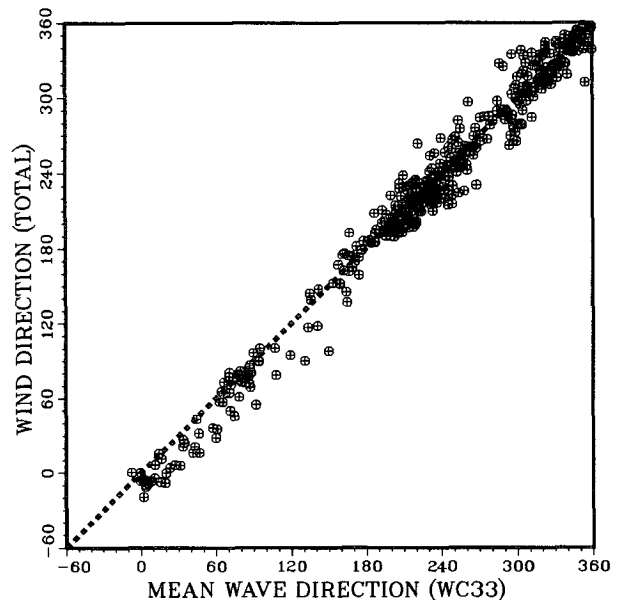

FIG. 3. Wind direction measured at the MINIMET as a function of the high frequency wave direction defined by Eq. (4.1) measured at WAVEC33 in degrees true, for $\mathcal{U} \geqslant 5$ m s^{-1}. Perfect agreement is shown by the dashed line. Offshore, onshore, and alongshore wind directions are included.

TABLE 1. Correlation coefficient $\mathcal{R}$ and rms errors comparing the wave direction as calculated from Eq. (4.1) for the directional buoys with the wind direction at the MINIMET. Number of points is given by $\mathcal{N}$.

| Buoy | Only winds > 5 m s^{-1} | | | All winds | | |
	$\mathcal{R}$	Rms error (deg)	$\mathcal{N}$	$\mathcal{R}$	Rms error (deg)	$\mathcal{N}$
WAVEC31	0.988	14.74	602	0.982	18.70	802
WAVEC32	0.992	11.64	622	0.989	13.82	810
WAVEC33	0.989	13.57	476	0.985	16.27	640

5 m s^{-1} are not included in the analysis. The agreement is almost perfect.

Correlation coefficients, presented in Table 1 for all three buoys, are 0.99 with rms errors less than 14.7°. Marsden and Juszko (1989) time series analysis from the Grand Banks gives a correlation coefficient of 0.99 and rms error 8.0°. Alongshore directions, particularly at approximately 70° and 250° true, result in deviations of the high frequency mean wave direction compared to the measured wind direction. Although these are only very slight in Fig. 3, they are evident at the other two buoys, which are closer to the shoreline (not shown). The deviations represent the effects of the very jagged Nova Scotian coastline on the wind-generated waves. They are limitations on the estimation of offshore winds from fetch-limited waves. Table 1 shows that when all wind speeds are included in the analysis, we obtain correlation coefficients of about 0.99 and slightly larger rms errors. This demonstrates that the direction of the high-frequency equilibrium region of the spectrum, derived from the quadspectra Q_{12} and Q_{13}, provides a good measure of the observed wind direction.

5. Onshore winds

When the wind is onshore, there is no roughness change such as occurs at the land–water boundary in the offshore case, in the sense that no boundary-layer height adjustment occurs over water. The waves are therefore similar to those of the open ocean. Conditions are approximately equivalent to the Marsden and Juszko (1989) directional buoy data from the Grand Banks or to that of any other observation point in the open ocean.

Our analysis considers situations where the winds are within a window of ±60° to orthogonal from the coast to eliminate contamination due to winds interacting with the irregular coastline, as noted in section 4. We include as wide a window as possible to maximize the size of our dataset. For offshore situations considered in the next section, it is necessary to consider a narrow window because otherwise the fetch becomes

noisy due to the jagged coastline. We present the wind speed measured at the meteorological buoy as a function of the total $E_2 + E_3$ wave slope $\langle k^2 \rangle E_0$ for the outermost wave buoy in Fig. 4. Results for E_2 and E_3, and also at the other two wave buoys, are similar. An empirical fit between $\mathcal{U}$ and wave slope $\langle k^2 \rangle E_0$, denoted s, was computed using the parameterization,

$$\mathcal{U} = \mathcal{A}_0 + \mathcal{A}_1 s + \mathcal{A}_2 s^2. \qquad (5.1)$$

Results are reported in Table 2, including error estimates for $\mathcal{A}_0$ and $\mathcal{A}_1$ and correlation coefficients $\mathcal{R}$. The units of $\mathcal{A}_0$, $\mathcal{A}_1$, and $\mathcal{A}_2$ are meters per second. Marsden and Juszko (1989) results, showing slightly smaller correlation coefficients and higher rms errors, are reported in Table 3 and Fig. 4.

The quadratic term in Eq. (5.1) is used to provide a best fit between wave slope and wind speed. Section 2 suggested that the theoretical relation between wind speed and wave slope, as presented in Eq. (2.16), is essentially linear. The quadratic term represents the higher-order dependence inherent in the f_p^* terms of the coefficients of Eq. (2.16). Table 2 affirms that the quadratic term has a minor role: when it is combined with typical values for wave slope $\langle k^2 \rangle E_0$ measured by the buoy, as shown in Fig. 4, the resultant contribution is much smaller than that of the first two terms of Eq. (5.1).

Under onshore conditions, it is clear from the geometry of the jagged Nova Scotian coastline shown in Fig. 1 that the E_2 (north–south) spectral components and the E_3 (east–west) spectral components are composed of upwind and crosswind components. Table 2
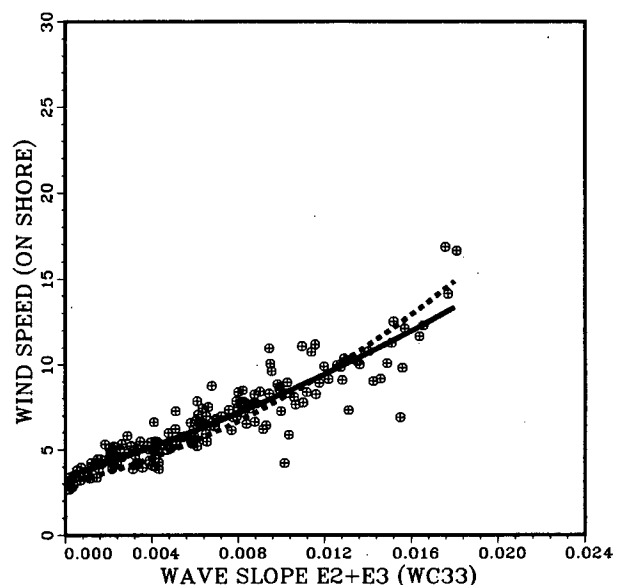

FIG. 4. Wind speed (m s^{-1}) at 10 m as a function of total wave slope $E_2 + E_3$ for onshore ±60° winds at the outermost wave buoy of the array, with least squares fit shown by solid line and Marsden and Juszko (1989) dashed line.

TABLE 2. Quadratic parameterizations given by Eq. (5.1), correlation coefficients $\mathcal{R}$, and rms errors for wind speed as a function of the north–south E_2, the east–west E_3, and the total $E_2 + E_3$ wave slope for onshore ($\pm 60°$) winds as presented in Fig. 4. Errors in the $\mathcal{A}_0$ and $\mathcal{A}_1$ coefficients are indicated by $\pm\Delta\mathcal{A}_0$ and $\pm\Delta\mathcal{A}_1$. Number of points is given by $\mathcal{N}$.

| | WAVEC31 | | | WAVEC32 | | | WAVEC33 | | |
| | $\mathcal{N} = 128$ | | | $\mathcal{N} = 176$ | | | $\mathcal{N} = 140$ | | |
	E_2	E_3	$E_2 + E_3$	E_2	E_3	$E_2 + E_3$	E_2	E_3	$E_2 + E_3$
$\mathcal{A}_0$	3.29	3.00	3.07	3.32	2.60	2.80	3.61	3.23	3.46
$\mathcal{A}_1$	1170.9	1453.9	621.43	1198.6	1706.0	734.60	748.07	1137.6	393.47
$-\mathcal{A}_2$	6676.8	20718.	−570.71	24380.	71653.	11273.	−25384.	16592.	−8646.5
$\mathcal{R}$	0.92	0.88	0.93	0.88	0.84	0.88	0.89	0.87	0.91
rms	1.26	1.56	1.23	1.50	1.68	1.49	1.19	1.25	1.03
$\pm\Delta\mathcal{A}_0$	±0.16	±0.23	±0.15	±0.22	±0.33	±0.25	±0.14	±0.22	±0.12
$\pm\Delta\mathcal{A}_1$	±55.24	±89.5	±28.6	±72.5	±125.2	±45.0	±60.0	±96.6	±26.8

shows that it is possible to correlate onshore winds to the E_2 (north–south) spectral data and the E_3 (east–west) spectral data. The resultant correlation coefficients are significant and comparable to the correlations for $E_2 + E_3$. This verifies Eqs. (2.17)–(2.18), that E_2 and E_3 components of spectral wave slope lead to wave age–dependent relations between wind speed and wave slope, which are analogous to Eq. (2.16).

6. Offshore winds

a. Winds as a function of wave slope

When the wind is offshore, there is a change in roughness at the land–water boundary. In fact, before the winds pass over the water, they pass over forest, swamp, and low hills, according to the trajectory that they follow at a given instant, and these factors contribute to the effective boundary-layer roughness that shapes the wind field that finally reaches the water, as discussed in Dobson et al. (1989). At the land–water boundary, the roughness changes once more and an associated boundary-layer height adjustment occurs. The wind speed profile for fetch-limited wind-generated waves is therefore highly variable for differing slanting fetch situations in the offshore case.

To correlate wind speed and the wave slope we restrict our attention to situations where the winds are within $\pm 30°$ to orthogonal from the coastline to eliminate contamination from slanting fetch cases. We also require that the wind direction as measured at the shoreline be within $\pm 15°$ of the high frequency wave direction determined by Eq. (4.1), to ensure that the

wave directions have relaxed to the wind direction. Figure 5 and Table 4 present wind speed, as measured at the meteorological buoy, as a function of the north–south (E_2) wave slope from the outermost wave buoy. Results for east–west E_3 and total $E_2 + E_3$ wave slope are similar. Figure 6 verifies that the time series of measured offshore wind speeds at the meteorological buoy is in good agreement with the wind speeds derived from the wave slopes measured at WAVEC33. Moreover, the corresponding case, when the wind direction as measured at the shoreline is within $\pm 10°$ of the high frequency wave direction, is similar, as shown in Table 4. This demonstrates that the calibration is stable with respect to small variations in the high frequency wave direction, compared to the wind direction.
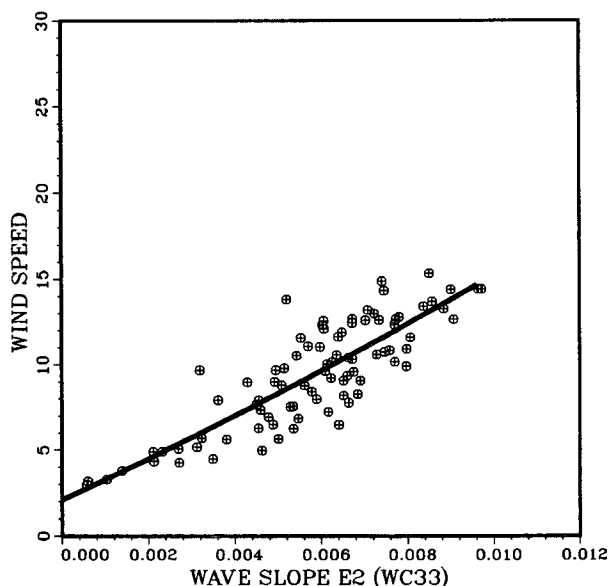
TABLE 3. As in Table 2, from Marsden and Juszko (1989). The number of points is 272.

	Upwind wave slope	Crosswind wave slope	Total wave slope $(E_2 + E_3)$
$\mathcal{R}$	0.90	0.84	0.88
rms	1.9	2.3	2.0

FIG. 5. Wind speed (within $\pm 30°$ offshore to orthogonal to the shoreline) measured at the meteorological buoy, as a function of north–south wave slope E_2 measured at the outermost wave buoy of the array. Shoreline wind directions are required to be within $\pm 15°$ of high-frequency wave directions. Least squares parameterization as given in Table 4 is shown by solid line.

TABLE 4. As in Table 2 for offshore ±30° winds with shoreline winds within ±10° and ±15° to the high frequency wave directions for WAVEC33. The ± 15° case is presented in Fig. 5 for E_2. Number of points is given by $\mathcal{N}$.

	±10° $\mathcal{N} = 64$			±15° $\mathcal{N} = 95$		
	E_2	E_3	$E_2 + E_3$	E_2	E_3	$E_2 + E_3$
$\mathcal{A}_0$	2.08	2.90	2.62	2.09	3.04	2.75
A_1	1129.5	1018.2	410.39	1172.3	986.72	415.87
A_2	1.6×10^4	8.9×10^4	2.1×10^4	1.4×10^4	9.3×10^4	2.1×10^4
$\mathcal{R}$	0.82	0.83	0.86	0.85	0.86	0.88
rms	1.73	1.66	1.54	1.66	1.59	1.47

Identifying coefficients $\mathcal{A}_0$ and $\mathcal{A}_1$ from Table 4 with coefficients $\mathfrak{C}_3$ and $\mathfrak{D}_3$ in Eq. (2.19a), we iteratively solve Eq. (2.21) and therefore determine Γ_{23}. Knowing Γ_{23}, we evaluate $\mathfrak{C}_2$ and $\mathfrak{D}_2$ from Eq. (2.20) and estimate $\mathcal{U}_2$ as a function of wave slope from Eq. (2.19b). This establishes a calibration of wind speed with wave slope at the middle wave buoy. Equations for Γ_{13} and $\mathcal{U}_1$ may be treated similarly. As an example, assuming the wind speed at the outermost end of the wave buoy array is either 10 or 15 m s^{-1}, the corresponding relations between wind speed and wave slope at the other two wave buoys are presented in Fig. 7a. Table 4 implies an rms error in estimated wind speed of about 1.5 m s^{-1} in Fig. 7a, assuming the level of error is constant for all wind speeds. It follows that verification of the calibrations of wind speed with wave slope at WAVEC32 and WAVEC31, as displayed in Fig. 7a, may not be possible using wave buoy measurements.

The profile of wind speed as a function of fetch resulting from Smith and MacPherson (1987) was not stratified as a function of wind speed, but represents a composite of all observations. Therefore, the calibration of wind speed with wave slope, as expressed by measured values for $\mathfrak{C}_3$ and $\mathfrak{D}_3$ in Eq. (2.19a), is a composite calibration for the outermost wave buoy and, as a result, only one wind speed–wave slope curve is possible in Fig. 7a, for the outermost wave buoy. Families of wind speed–wave slope curves, represented by 10 and 15 m s^{-1}, result at the other two wave buoys as a consequence of the dependency on wind speed and wave age in Eqs. (2.19)–(2.20). Moreover, these families exhibit nonparallel behavior, which is mostly due to the C_{d2}/C_{d3} terms in Eqs. (2.19)–(2.20). Were it not for this C_{d2}/C_{d3} dependence, the families of curves would be essentially parallel, as shown in Fig. 7b.

b. The variation of wind with fetch

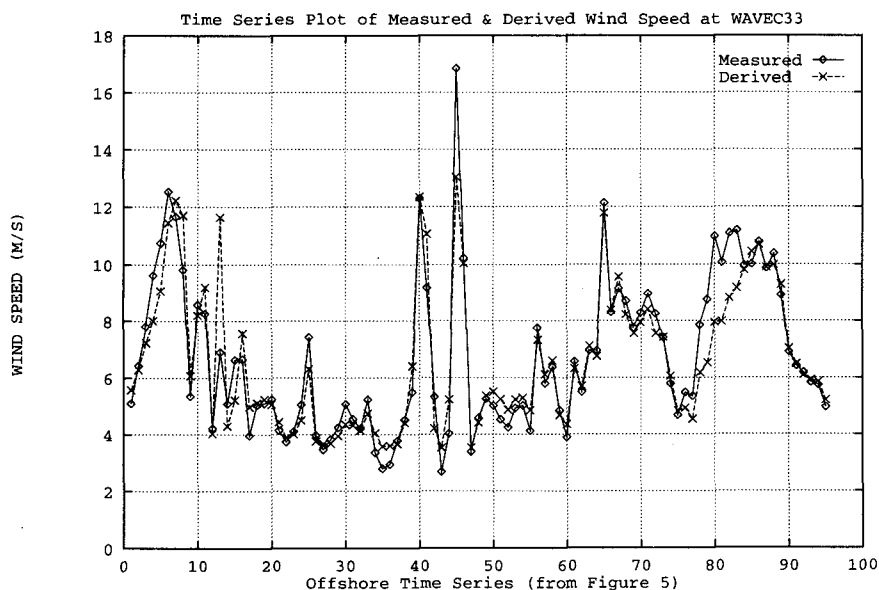There are very few measurements of the variation of surface wind speed as a function of fetch for offshore

FIG. 6. Time series of offshore winds measured at the meteorological buoy and derived from the calibrated wave slopes at the outermost wave buoy, for the duration of the CASP experiment. Gaps for onshore and alongshore wind directions have not been included.
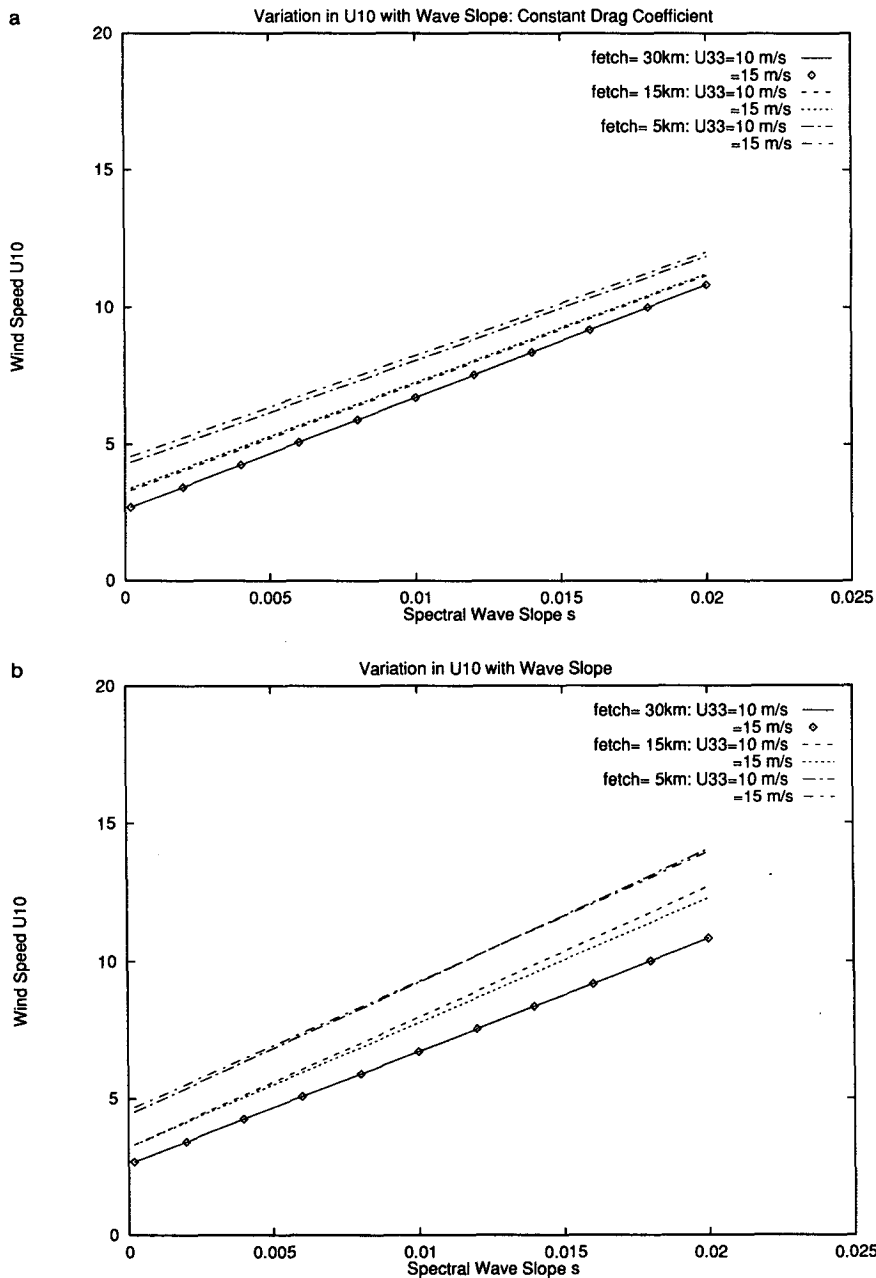
a

b

FIG. 7. (a) Wind speed as a function of wave slope at the three wave buoys when $\mathcal{U}_3$ is 10 and 15 m s^{-1}. (b) Neglecting the (C_{d2}/C_{d3}) terms in Eqs. (2.19)–(2.21).

winds. Smith and MacPherson (1987) achieved a set of aircraft observations at 50-m height. Assuming a logarithmic profile, these may be reduced to in situ winds U at 10 m height, and Dobson et al. (1989) show that they compare well with the modeling guidelines of Taylor and Lee (1984). Although the Smith and MacPherson data is unique, the error bars are quite large. It is therefore important to have further analyzed observations to give insight into the wind profile as a function of fetch.

For offshore winds, we generalize Eq. (2.21)

$$\Gamma_x = \left(\mathfrak{S}_3 \left(\frac{X}{X_3} \right)^b \left(\frac{C_{dx}}{C_{d3}} \right)^{-(1/2)-b} \Gamma_x^{-2b} \right.$$

$$\left. + \mathfrak{D}_3 \left(\frac{X}{X_3} \right)^{-ab} \left(\frac{C_{dx}}{C_{d3}} \right)^{ab-(1/2)} \Gamma_x^{2ab} s \right) \mathcal{U}_3^{-1}, \quad (6.1)$$

where X is the fetch from the shoreline, C_{dx} is the drag coefficient at fetch X, and $\Gamma_x \equiv \mathcal{U}_x / \mathcal{U}_3$. Knowing the

wave slope s at all the wave buoys and the wind speed $\mathcal{U}_3$ at the outermost wave buoy and assuming a simple interpolation for s, we solve Eq. (2.21) and thereby determine the linearly averaged wind speed profile as a function of fetch. Figure 8a presents the resultant wind profiles assuming that, at 50 km, $\mathcal{U} = 10$, 12, and 15 m s^{-1}. It is evident that as wind speed increases, the variation in the wind speed profile also increases.

Smith and MacPherson (1987) found the empirical wind profile (normalized to the winds at 50 km fetch from the shoreline) at 10-m height,

$$U(x) = U_{50 \text{ km fetch}}(1 - 0.27 e^{-x/9.3}), \quad (6.2)$$

as a composite profile for all measured wind speeds in the range from 9 to 15 m s^{-1}, where x is in units of kilometers. This relation was found for conditions of
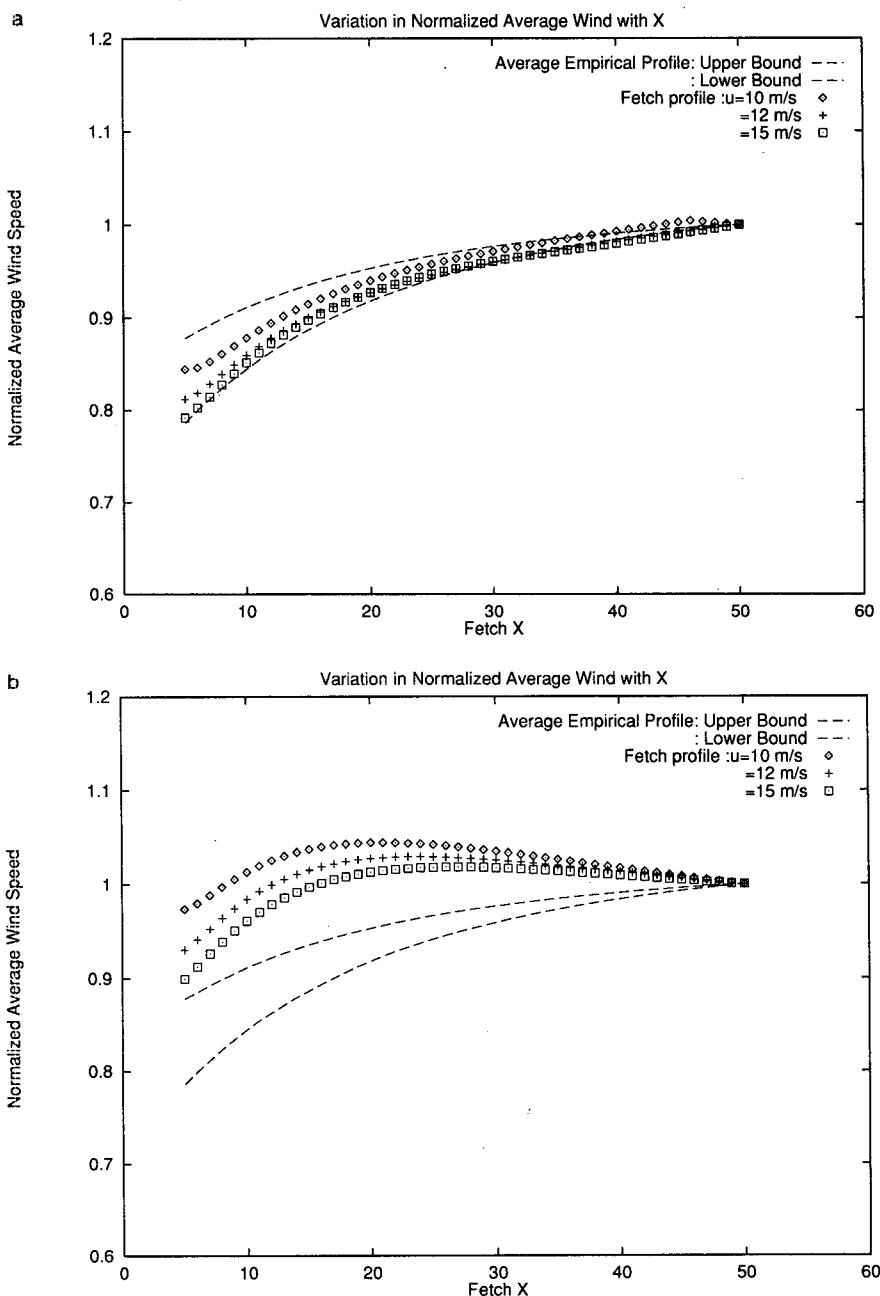
FIG. 8. (a) Estimation of the linearly averaged wind speed profile $\mathcal{U}$ as a function of fetch X, as determined from Eq. (6.1), assuming for example $\mathcal{U}_3 = 10$, 12, and 15 m s^{-1}. Upper and lower bounds for the linearly averaged empirical wind speed profile from Smith and MacPherson (1987) are shown as (---). (b) Assuming constant drag coefficient $C_d|_{\text{const}}$ and associated CASP fetch laws.

cold offshore winds, when the mean wind is dominated by changes to surface roughness rather than surface temperature or heat flux contrast. Dobson et al. (1989) present an alternate model for the wind speed profile, using the Taylor and Lee (1984) guidelines, that is largely in agreement with the Smith and MacPherson (1987) empirical relation and will not be presented here. Appropriate comparisons between Smith and MacPherson (1987) and Taylor and Lee (1984) are given in Dobson et al. (1989). The linear fetch average of the Smith and MacPherson empirical fit, given by Eq. (6.2), is computed via

$$\mathcal{U} = \frac{1}{x} \int_0^x U(x) dx. \qquad (6.3)$$

This is presented in Fig. 8a and agrees well with the wind speeds inferred from wave slopes, from Eq. (6.1). The wave age dependency in the formulation for the drag coefficient $C_d|_{\text{HEXOS}}$ in Eq. (2.24) is important in achieving estimates for the variation of wind speed with fetch that agree with Smith and MacPherson (1987). Figure 8b shows the wind variation with fetch resulting from the CASP fetch relations with an assumed constant drag coefficient $C_d|_{\text{const}}$. In this case, the agreement with the Smith and MacPherson observations is poor.

Upper and lower bounds on the mean wind profile per se are presented in Figs. 8a–b. These bounds were obtained as a consequence of the guidelines of Taylor and Lee (1984) and the variation in surface roughness between forest, swamp, and low hills at the shoreline, following Dobson et al. (1989). The error in the mean wind profile described by Eqs. (6.2)–(6.3), resulting from measurements by Smith and MacPherson (1987), is about ±0.05. On the other hand, the rms error for each wind speed estimate from Table 4 is about 1.5 m s^{-1}. Therefore, a wind speed of 10 m s^{-1} would have to decrease to a normalized value of 0.85 for the observed decrease to be significant. A wind speed of 15 m s^{-1} would have to decrease to a normalized value of 0.9 to be significant. As this is attained in Fig. 8a, the theoretical estimates for the wind speed variation with fetch may be verified from wave buoy data.

7. Concluding discussion

We have derived a relation for wind speed $\mathcal{U}$ (and friction velocity $\mathcal{U}^*$) in terms of spectral wave parameters such as dimensionless frequency f_p^*, the Phillips (1958, 1985) α coefficient, and wave slope $\langle k^2 \rangle E_0$. The key to the derivation is the evaluation of one-dimensional spectral energy $E(f)$ in terms of a simple parametric form involving α, which we invert and average over the high frequency region of the equilibrium range. Thus, using Eq. (2.5), α is computed and related to the peak frequency f_p and to wave slope components, denoted $\langle k^2 \cos^2\theta \rangle E_0$, $\langle k^2 \sin^2\theta \rangle E_0$, and $\langle k^2 \rangle E_0$. The fetch relations (2.6) for growing waves then lead to a

determination of wind speed in terms of wave slope s and wave age, Eq. (2.16).

The relation (6.1) between wind speed and spectral wave parameters may be generalized as

$$\Gamma_x = \left(\mathbb{S}_\infty \left(\frac{X}{X_\infty} \right)^b \left(\frac{C_{dx}}{C_{d\infty}} \right)^{(1/2)b} \Gamma_x^{-2b} \right.$$
$$\left. + \mathbb{D}_\infty \left(\frac{X}{X_\infty} \right)^{-ab} \left(\frac{C_{dx}}{C_{d\infty}} \right)^{ab(1/2)} \Gamma_x^{2ab} s \right) \mathcal{U}_\infty^{-1}, \qquad (7.1)$$

where X_∞ is the fetch necessary for the development of fully developed wind-generated waves, $C_{d\infty}$ is the open ocean long-fetch drag coefficient, and $\Gamma_x \equiv \mathcal{U}_x / \mathcal{U}_\infty$. This specifies the wind speed as a function of fetch X and wave slope s, given the wind speed $\mathcal{U}_\infty$ at fetch X_∞. From Table 2, which is valid for onshore wind conditions and therefore approximates open ocean long-fetch conditions, we estimate that $\mathbb{S}_\infty \approx 3.5$ and $\mathbb{D}_\infty \approx 390$. Equations for E_2 or E_3 would use different values for $\mathbb{S}_\infty$ and $\mathbb{D}_\infty$, as discussed in Eqs. (2.17)–(2.18) and involve constants $\mathcal{P}_s$ and $\mathcal{P}_c$. In terms of dimensionless peak frequency f_p^* and the Phillips α coefficient at fetch X, this equation may be rewritten in terms of open ocean (no explicit fetch) parameters,

$$\mathcal{U}_x^* = \mathbb{S}_\infty f_p^* / f_{p\infty}^* + \mathbb{D}_\infty \alpha_\infty / \alpha s. \qquad (7.2)$$

Moreover, Eq. (7.2) follows directly from Eq. (2.15) without any assumption about the variation of the drag coefficient C_d as the spectrum evolves. Knowing the wave slope, denoted $\langle k^2 \rangle E_0$ or s, and spectral wave parameters such as dimensionless peak frequency f_p^* and Phillips α coefficient, Eq. (7.2) leads directly to the friction velocity $\mathcal{U}^*$. Using measurements of friction velocity $\mathcal{U}^*$ and wave slope s from the Grand Banks ERS-1 Calibration/Validation Experiment of Dobson et al. (1994), a related paper is being prepared to verify Eq. (7.2).

Equation (7.1) was verified with the CASP data of Dobson et al. (1989). Wave buoy measurements (at the seaward end of the buoy array) were first calibrated with in situ offshore wind observations. Thus having calibrated wind speed to wave slope $\langle k^2 \rangle E_0$, the wind speed was inferred at the other two wave buoys within the array. Knowing the wave slope s at all wave buoys and the wind speed $\mathcal{U}$ at the outermost wave buoy, we thereby determine the wind speed $\mathcal{U}$ as a function of fetch. It is essential, however, to use the sea state–dependent drag coefficient in conjunction with fetch-growth relations that also assume sea state dependence in the drag coefficient to use the buoy-measured wave slopes to infer wind speed. We used the fetch-growth relations from the CASP data from Perrie and Toulany (1990), which assumed sea state dependence in the drag coefficient $C_d|_{\text{HEXOS}}$, and we also used the same drag coefficient $C_d|_{\text{HEXOS}}$ to get the estimated fetch variation of the wind speed (Fig. 8a). The resulting
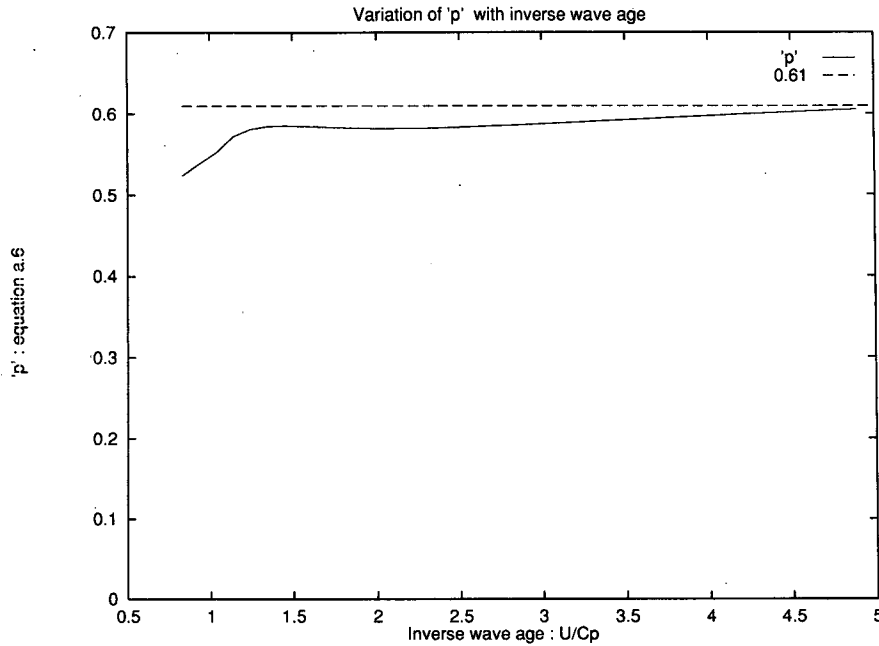
FIG. 9. Variation of p from Eq. (A.6) as a function of $\mathcal{U}/\mathcal{C}_p$.

comparison with Smith and MacPherson (1987) measurements is good. When fetch-growth relations are used assuming a constant drag coefficient $C_d|_{\text{const}}$, estimated wind speeds compare poorly with Smith and MacPherson.

APPENDIX

On the Equilibrium Range

We present an argument that $\mathcal{J}$, defined in Eq. (2.11) as

$$\mathcal{J} = \frac{(E_0)_{\text{eq.ra.}}\langle f^4 \rangle_{\text{eq.ra.}}}{E_0 \langle f^4 \rangle}, \qquad \text{(A.1)}$$

is approximately constant. The one-dimensional wave spectrum parameterization of Hasselmann et al. (1973) may be written as

$$E(f) = \alpha g^2 (2\pi)^{-4} f^{-5} \exp\left\{-\frac{5}{4}(f_p/f)^4\right\}\gamma^{\Gamma}\Lambda(\theta),$$
$$\text{(A.2)}$$

where

$$\Gamma = \exp\{-(f - f_p)^2/2\sigma^2 f_p^2\}, \qquad \text{(A.3)}$$

γ is the peak enhancement factor, and σ the peak width parameter. For wind-generated waves in the absence of swell (in which case $f_s = 0$), $\mathcal{J}$, as defined in Eq. (A.1), is explicitly

$$\mathcal{J} = \frac{\displaystyle\int_{1.5 f_p}^{f_N} \alpha g^2 (2\pi)^{-4} f^{-1} \exp\left\{-\frac{5}{4}(f_p/f)^4\right\}\gamma^{\Gamma} df}{\displaystyle\int_0^{f_N} \alpha g^2 (2\pi)^{-4} f^{-1} \exp\left\{-\frac{5}{4}(f_p/f)^4\right\}\gamma^{\Gamma} df}.$$
$$\text{(A.4)}$$

Rewriting the integral on interval $[0, f_N]$ as the sum of integrals on $[0, 3/2 f_p]$ and $[3/2 f_p, f_N]$, representing f_N as about $3 f_p$ as suggested by Donelan et al. (1985) and making a change of variables, Eq. (A.4) simplifies to

$$\mathcal{J} = 1/(1 + p), \qquad \text{(A.5)}$$

where

$$p = \frac{\displaystyle\int_0^{3/2} \frac{1}{u} e^{-(1/u)^2}\gamma^{\exp[-(u-1)^2/2\sigma^2]} du}{\displaystyle\int_{3/2}^4 \frac{1}{u} e^{-(1/u)^2}\gamma^{\exp[-(u-1)^2/2\sigma^2]} du}. \qquad \text{(A.6)}$$

As stated by Hasselmann et al. (1976), there is only a very small discernable trend in the behavior of the spectral parameters γ and σ as the spectrum evolves. More recently, Donelan et al. (1985) present param-

eterizations for γ and σ as functions of inverse wave age, defined in terms of wind speed $\mathcal{U}/\mathcal{C}_p$:

$$\gamma = \begin{cases} 1.7, & 0.83 < \mathcal{U}/\mathcal{C}_p < 1 \\ 1.7 + 6.0 \log(\mathcal{U}/\mathcal{C}_p), & 1 \leqslant \mathcal{U}/\mathcal{C}_p \leqslant 5 \end{cases}$$

(A.7)

and

$$\sigma = 0.08[1 + 4/(\mathcal{U}/\mathcal{C}_p)^3],$$

$$0.83 < \mathcal{U}/\mathcal{C}_p < 5.$$ (A.8)

We use these relations to compute p as a function of inverse wave age $\mathcal{U}/\mathcal{C}_p$ as presented in Fig. 9 Thus, we verify that $\mathcal{J}$ is approximately constant, which supports the Hasselmann et al. (1976) suggestion.

REFERENCES

Chalikov, D., 1995: The parameterization of the wave boundary layer. *J. Phys. Oceanogr.,* in press.

——, and M. Yu. Belevich, 1993: One-dimensional theory of the wave boundary layer. *Bound.-Layer Meteor.,* **63,** 65–96.

Cox, C., and W. Munk, 1954a: Statistics of the sea surface derived from sun glitter. *J. Mar. Res.,* **13,** 198–227.

——, and ——, 1954b: Measurements of the roughness of the sea surface from photographs of the sun's glitter. *J. Opt. Soc. Amer.,* **44,** 838–850.

Dobson, F., W. Perrie, and B. Toulany, 1989: On the deep-water fetch laws for wind-generated surface gravity waves. *Atmos.-Ocean,* **27**(1), 210–236.

——, S. D. Smith, R. J. Anderson, P. W. Vachon, D. Vandemark, J. R. Buckley, M. Allingham, M. Kandekar, and R. Lalbeharry, 1994: The Grand Banks *ERS-1* SAR Wave Experiment. *Eos, Trans. Amer. Geophys. Union,* **74**(4), 41 and 44–45.

Donelan, M. A., J. Hamilton, and W. H. Hui, 1985: Directional spectra of wind-generated waves. *Philos. Trans. Roy. Soc. London, A* **315,** 509–562.

Hasse, L., M. Grünewald, and D. E. Hasselmann, 1978: Field observations of air flow over waves. *Turbulent Fluxes through the Sea Surface, Wave Dynamics and Prediction.* A. Favre and K. Hasselmann, Eds., Plenum, 483–494.

Hasselmann, K., T. P. Barnett, E. Bouws, H. Carlson, D. E. Cartwright, K. Enke, J. A. Ewing, H. Gienapp, D. E. Hasselmann, P. Kruseman, A. Meerburg, P. Müller, D. J. Olbers, K. Richter, W. Sell, and H. Walden, 1973: Measurements of wind-wave growth and swell decay during the Joint North Sea Wave Project (JONSWAP). *Dtsch. Hydrogr. Z., Erganzungsheft Reihe A* (8°), 12, 95 pp.

——, D. B. Ross, P. Müller, and W. Sell, 1976: A parametric wave prediction model. *J. Phys. Oceanogr.,* **6,** 200–228.

Hasselmann, S., and K. Hasselmann, 1981: A symmetrical method of computing the nonlinear transfer in a gravity-wave spectrum. *Hamburger Geophys. Einzelschr., A* **52,** 163 pp.

Janssen, P. A. E. M., 1989: Wave-induced stress and the drag of air flow over sea waves. *J. Phys. Oceanogr.,* **19,** 745–754.

——, 1991: Quasi-linear theory of wind-wave generation applied to wave forecasting. *J. Phys. Oceanogr.,* **21,** 1631–1642.

——, and P. Woiceshyn, 1991: Wave age and the scatterometer wind retrieval algorithm. ESA Report on CALVAL Workshop, Penhorse, France, 141–145.

Jenkins, A. D., 1992: A quasi-linear eddy viscosity model for the flux of energy and momentum to wind waves using conservation-law equations in a curvilinear coordinate system. *J. Phys. Oceanogr.,* **22,** 842–858.

Longuet-Higgins, M. S., D. E. Cartwright, and N. D. Smith, 1963: Observations of the directional spectrum of sea waves using the motions of a floating buoy. *Proc., Ocean Wave Spectra Proc. Conf.,* Easton, MD, U.S. Naval Oceanographic Office, 111–136.

Marsden, R. F., and B.-A. Juszko, 1989: Wind estimates from wave slopes. *J. Geophys. Res.,* **94**(C5), 6266–6272.

Perrie, W., and B. J. Toulany, 1990: Fetch relations for wind-generated waves as a function of wind-stress scaling. *J. Phys. Oceanogr.,* **20,** 1666–1681.

Phillips, O. M., 1958: The equilibrium range in the spectrum of wind-generated ocean waves. *J. Fluid Mech.,* **4,** 426–434.

——, 1985: Spectral and statistical properties of the equilibrium range in wind-generated gravity waves. *J. Fluid Mech.,* **156,** 505–531.

Resio, D., and W. Perrie, 1989: Implications of an f^{-4} equilibrium range for wind-generated waves. *J. Phys. Oceanogr.,* **19,** 193–204.

——, and ——, 1991: A numerical study of nonlinear energy fluxes due to wave–wave interactions. Part I: Methodology and basic results. *J. Fluid Mech.,* **223,** 603–629.

Smith, P. C., and J. I. MacPherson, 1987: Cross-shore variations of near-surface wind velocity and atmospheric turbulence at the land–sea boundary during CASP. *Atmos.-Ocean,* **25,** 279–303.

Smith, S. D., 1981: Coefficients for sea-surface wind stress and heat exchange. Bedford Institute of Oceanography Rep. BI-R-81-19, 31 pp.

——, 1988: Coefficients for sea surface wind stress, heat flux, and wind profiles as a function of wind speed and temperature. *J. Geophys. Res.,* **93,** 15 467–15 472.

——, and R. J. Anderson, 1989: Eddy flux measurements during HEXMAX. *Proc. NATO Advanced Workshop on Humidity Exchange over the Sea: Main Experiment (HEXMAX) Analysis and Interpretation.* Tech. Rep., Dept. of Atmospheric Science, University of Washington, HEXOS Contrib. No. 16, 14–21.

——, ——, W. A. Oost, C. Kraan, N. Maat, J. DeCosmo, K. B. Katsaros, K. L. Davidson, K. Bumke, L. Hasse, and H. M. Chadwick, 1992: Sea surface wind stress and drag coefficients: The HEXOS results. *Bound.-Layer Meteor.,* **60,** 109–142.

Taylor, P. A., and R. J. Lee, 1984: Simple guidelines for estimating wind speed variations due to small-scale topographic features. *Climatol. Bull.,* **18,** 3–32.

Woiceshyn, P., and P. Janssen, 1991: Sensitivity study—Scatterometer retrievals with wave age parameter. ESA Report on CALVAL Workshop, Penhorse, France, 133–139.